I. Makkonen, M. Hakala, and M. J. Puska, Modeling the momentum distributions of annihilating electron-positron pairs in solids, Physical Review B 73, 035103: 1-12 (2006).

Modeling the momentum distributions of annihilating electron-positron pairs in solids

I. Makkonen,[1,*] M. Hakala,[2] and M. J. Puska[1]

[1]*Laboratory of Physics, Helsinki University of Technology, P.O. Box 1100, FI-02015 HUT, Finland*
[2]*Division of X-Ray Physics, Department of Physical Sciences, P.O. Box 64, FI-00014 University of Helsinki, Finland*

Measuring the Doppler broadening of the positron annihilation radiation or the angular correlation between the two annihilation gamma quanta reflects the momentum distribution of electrons seen by positrons in the material. Vacancy-type defects in solids localize positrons and the measured spectra are sensitive to the detailed chemical and geometric environments of the defects. However, the measured information is indirect and when using it in defect identification comparisons with theoretically predicted spectra is indispensable. In this article we present a computational scheme for calculating momentum distributions of electron-positron pairs annihilating in solids. Valence electron states and their interaction with ion cores are described using the all-electron projector augmented-wave method, and atomic orbitals are used to describe the core states. We apply our numerical scheme to selected systems and compare three different enhancement (electron-positron correlation) schemes previously used in the calculation of momentum distributions of annihilating electron-positron pairs within the density-functional theory. We show that the use of a state-dependent enhancement scheme leads to better results than a position-dependent enhancement factor in the case of ratios of Doppler spectra between different systems. Further, we demonstrate the applicability of our scheme for studying vacancy-type defects in metals and semiconductors. Especially we study the effect of forces due to a positron localized at a vacancy-type defect on the ionic relaxations.

I. INTRODUCTION

Positron annihilation spectroscopy[1] is an experimental method for studying electronic structures of materials. In comparison with other techniques to measure electron momentum densities such as $(e, 2e)$ spectroscopy[2] or Compton scattering[3] (to which we have already applied the same all-electron method as used in this work[4]) positron annihilation is characterized with the strong sensitivity to the vacancy-type defects, which makes it a method widely suitable in materials science and materials technology studies. In the crystal lattice positrons get trapped at possibly existing vacancy-type defects. By measuring positron lifetimes and momentum distributions of annihilating electron-positron pairs (angular correlation or Doppler broadening measurements of annihilation radiation) one obtains information about the open volumes and the chemical environments of the defects.

A successful use of positron annihilation measurements (in defect identification) calls for accompanying theoretical and computational work resulting in simulated annihilation characteristics to be compared with the measured ones (for a review see Ref. 5). In this paper we present a computational scheme based on the zero-positron-density $(n_+ \rightarrow 0)$ limit of the two-component density-functional theory[6] (TCDFT). We describe the valence electron states in materials using the projector augmented-wave (PAW) method,[7] which we have already used to simulate the electron momentum distributions measured by Compton scattering.[4] In the PAW method the core states are treated in the frozen-core approximation and described using atomic wave functions.[8] In this work, the positron state is solved in the real space using a Rayleigh quotient multigrid (RQMG) solver.[9] Our scheme gives good

results when compared to experiments for delocalized positron states, for which the $n_+ \rightarrow 0$ limit of the TCDFT is exact, as well as for positrons localized at vacancy-type defects.

The methods previously used in self-consistent calculations of electronic structures and wave functions for determination of momentum distributions of annihilating valence-electron-positron pairs include, for example, the pseudopotential method,[10–14] the full-potential linearized-augmented-plane-wave (FLAPW) method,[15–17] the linear muffin-tin orbital (LMTO) method[18] and localized basis set schemes.[19] Each of these methods has its own advantages and flaws. The FLAPW method, although being accurate, is computationally heavy and has a basis set that makes the momentum density calculations technically complicated. The pseudopotential method is efficient and simple to use in the momentum distribution calculations. The drawback is that one completely loses the information on the high-momentum Fourier components of the valence wave functions because soft pseudo wave functions are used in the calculation. The LMTO method has presentation problems in the interstitial regions, which renders it difficult to describe open structures such as vacancy-type defects and systems with low symmetry with it. The PAW method, in contrast, is as efficient as the ultrasoft pseudopotential method.[20] It can flexibly be used for the study of defects in solids including structural relaxation. The plane-wave representation of the pseudo wave functions makes things simple because plane-waves are eigenfunctions of the momentum. Moreover, the calculation of the PAW momentum density[4] is straightforward because the plane-waves extend also to the augmentation regions as opposed to the (L)APW method. Ishibashi has already applied the PAW method to the calculation of coincidence Doppler spectra for bulk materials,[21] and Uenodo *et al.* have used the same code to study vacancy-type defects in SiGe.[22] Pre-

viously, we have used the PAW scheme (without taking into account the effect of the positron-induced forces) to study vacancy-dopant complexes in highly Sb doped Si,[23] mono-vacancy in Al,[24] and to show that one can experimentally distinguish Ga vacancies (V_{Ga}) from V_{Ga}-O_N pairs in GaN.[25]

Many works, in which the interpretation of the results is based on the comparison between measured and simulated annihilation characteristics, have been published during the recent years. Therefore, a systematic study of the performance of different schemes and approximation is of utmost importance. Using the PAW method to describe the valence electrons and atomic orbitals for core electrons we test three different schemes and approximations to calculate momentum distributions of annihilating electron-positron pairs.

For the description of the many-body effects in the calculation of momentum distributions of annihilating electron-positron pairs we choose finally the so-called state-dependent scheme[8] and for annihilation rates within the state-dependent scheme the local-density approximation (LDA) enhancement factor parametrized by Boroński and Nieminen.[6] We show that use of the commonly used position-dependent enhancement factor leads to unphysical oscillations at high momenta when one considers ratios of Doppler spectra between two different materials. In the same way we compare the Boroński-Nieminen (BN) LDA to the generalized-gradient approximation (GGA) by Barbiellini *et al.*[26,27] Our results show that the BN-LDA describes the ratios more accurately compared with the experiment than the GGA. We also show that the ratios can be compared with the experiment reliably although the LDA enhancement overestimates the high-momentum region of the Doppler spectra arising from the annihilation with core electrons. There are no test systems solved theoretically (e.g., by the quantum Monte Carlo method) exactly enough to compare with.

When studying annihilation of positrons trapped at vacancies and comparing the results with experiments it is important to consider the effects of forces due to the localized positron on the ionic relaxation of the vacancy. The effects on calculated positron lifetimes and Doppler spectra are non-negligible. We study selected monovacancies in metals and semiconductors by including also the effects of the forces due to the localized positron.

The structure of the paper is as follows. In Sec. II we describe the computational method used. Section III presents results for bulk systems and Sec. IV selected results for vacancies in metals and semiconductors. Finally, we summarize our results and present conclusions in Sec. V.

II. THEORY AND COMPUTATIONAL METHODS

A. Calculation of the positron states

In our scheme we first calculate the self-consistent electronic structure of the system without the influence of the positron. Then we solve the positron state in the potential

$$V_+(\mathbf{r}) = \phi(\mathbf{r}) + V_{corr}(n_-(\mathbf{r})), \qquad (1)$$

where $\phi(\mathbf{r})$ is the Coulomb potential due to electrons and nuclei, $n_-(\mathbf{r})$ the electron density, and $V_{corr}(n_-(\mathbf{r}))$ is the n_+

$\rightarrow 0$ limit of the electron-positron correlation potential. Above, the self-interaction correction is explicitly made, i.e., since we are interested in the case of only one positron in the system, its self-direct Coulomb energy should exactly cancel its exchange-correlation energy. The calculation of the positron state is non-self-consistent because the effective potential for the positron [Eq. (1)] does not depend on the positron density.

The scheme described above is for a delocalized positron the exact $n_+ \rightarrow 0$ limit of the TCDFT but it has been proven appropriate in practice also in the case of localized positron states. In this connection it is often referred to as the "conventional scheme"[5] (CS). The approximation can be justified by considering the positron and its screening cloud as a neutral quasiparticle, which does not affect the average electron density. One of the difficulties in a full TCDFT calculation is that the electron-positron correlation functionals are poorly known at finite positron densities. The $n_+ \rightarrow 0$ limit used in the CS is known better.[28]

The thermalized positron in the lattice is in the $\mathbf{k}=0$ state. When studying bulk systems we calculate the positron wave function at the Γ point ($\mathbf{k}=0$). In the case of positrons localized at vacancies the energy eigenvalue corresponding to an isolated vacancy is broadened due to the supercell approximation to a narrow band of energies. We integrate over the lowest lying positron band by calculating the positron wave function both at the Γ point and at the Brillouin zone boundary point L and using the average of the respective results.[29]

B. Annihilation rate models

The positron lifetime τ is the inverse of the annihilation rate λ which in a given system is proportional to the overlap of the electron and positron densities

$$\lambda = \frac{1}{\tau} = \pi r_e^2 c \int d\mathbf{r}\, n_-(\mathbf{r})n_+(\mathbf{r})g(n_-(\mathbf{r}),n_+(\mathbf{r})). \qquad (2)$$

Above, r_e is the classical electron radius and c the speed of light. The enhancement factor $g(n_-(\mathbf{r}),n_+(\mathbf{r}))$ (the contact density or the electron-positron pair correlation function evaluated at the positron) takes into account the increase in the annihilation due to the screening cloud of electrons around the positron. [The corresponding result obtained by omitting this factor is called the independent-particle model (IPM) annihilation rate.] In the TCDFT and within the LDA g is written as a function of both the local electron and positron densities. In the CS $n_+ \rightarrow 0$ limit of the enhancement factor, denoted by $\gamma(n_-(\mathbf{r}))$, is used. Also Gilgien *et al.*[11] used the $n_+ \rightarrow 0$ limit of the enhancement factor in their calculations but they calculated the positron density self-consistently within the TCDFT. This scheme has been shown to lead to rather localized positron states and too low core electron annihilation rates in comparison with experiments.[12]

The enhancement factor in the Boroński-Nieminen two-component formalism[6] is based on the results of the many-body calculations by Lantto.[30] Gilgien *et al.*[11] and Barbiellini *et al.*[26,27] have used the $n_+ \rightarrow 0$ limit parametrizations consistent with the correlation energy results of Arponen and Pajanne.[28]

The LDA systematically underestimates positron lifetimes in materials because it overestimates the annihilation with core electrons for which the correlation effects are less important.[26,27] Therefore, Barbiellini *et al.*[26,27] have presented a gradient-corrected scheme in which the enhancement factor γ is interpolated between the LDA ($\gamma = \gamma_{\text{LDA}}$, zero gradient) and the IPM values ($\gamma \equiv 1$, infinite gradient) as a function of the charge density gradient ∇n_-. Effectively, the interpolation means that the annihilation with valence electrons in the interstitial region is described using the LDA but when the density gradient is high (as near nuclei where the rapid oscillations of core and valence wave functions take place) the enhancement factor decreases and approaches the IPM limit ($\gamma \equiv 1$). The interpolation form contains one semi-empirical parameter. The value $\alpha = 0.22$ has been found to give with the Arponen-Pajanne enhancement lifetimes in good agreement with the experiment.[26,27] One must note that also the correlation potential for the positron is gradient corrected in the scheme by Barbiellini *et al.* However, the different enhancement factors cause directly most of the differences compared to the BN-LDA. The LDA parametrization of the correlation potential is the same in both schemes.

C. Schemes for the calculation of momentum distributions of annihilating electron-positron pairs

The IPM formula for the momentum distribution of annihilating electron-positron pairs is written as

$$\rho(\mathbf{p}) = \pi r_e^2 c \sum_j \left| \int d\mathbf{r} e^{-i\mathbf{p}\cdot\mathbf{r}} \psi_+(\mathbf{r}) \psi_j(\mathbf{r}) \right|^2, \qquad (3)$$

where $\psi_+(\mathbf{r})$ and $\psi_j(\mathbf{r})$ are wave functions of the positron and the electron on orbital j, respectively. The summation goes over the occupied electron states. The IPM is often used because it gives, in contrast to the annihilation rate, a rather good qualitative correspondence (shape of the momentum distribution) with experiments. A common way to take into account the electron-positron correlation effects is to introduce in the IPM expression the position-dependent LDA enhancement factor $\sqrt{\gamma(n_-(\mathbf{r}))}$,[31]

$$\rho(\mathbf{p}) = \pi r_e^2 c \sum_j \left| \int d\mathbf{r} e^{-i\mathbf{p}\cdot\mathbf{r}} \psi_+(\mathbf{r}) \psi_j(\mathbf{r}) \sqrt{\gamma(n_-(\mathbf{r}))} \right|^2. \quad (4)$$

We call this the state-independent LDA scheme. Equation (4) is, at least in a homogeneous system, consistent with the total annihilation rate λ of Eq. (2). Namely, one should obtain λ by integrating over the momentum

$$\lambda = \int d\mathbf{p} \rho(\mathbf{p}). \qquad (5)$$

The state-independent LDA scheme is motivated by the enhancement factor of the contact density, but it is not obvious how the screening really modifies the (electron) wave function. One can consider the position-dependent enhancement factor $\sqrt{\gamma(n_-(\mathbf{r}))}$ as a factor describing the distortion of the two-body wave function $\psi_+(\mathbf{r}) \psi_j(\mathbf{r})$ (where both the electron and the positron reside at the same point) due to the short-

range electron-positron correlation. What is problematic is that the two-body wave function is distorted *everywhere* at the instant of the annihilation although the screening is a local phenomenon. This causes the correlation effects to be overestimated in the state-independent LDA scheme.

In the so-called state-dependent scheme[8] a constant electron-state-dependent enhancement factor γ_j is used, i.e.,

$$\rho(\mathbf{p}) = \pi r_e^2 c \sum_j \gamma_j \left| \int d\mathbf{r} e^{-i\mathbf{p}\cdot\mathbf{r}} \psi_+(\mathbf{r}) \psi_j(\mathbf{r}) \right|^2. \quad (6)$$

The enhancement factor is written as $\gamma_j = \lambda_j / \lambda_j^{\text{IPM}}$, where λ_j is the annihilation rate of the state j within the LDA or the GGA,

$$\lambda_j = \pi r_e^2 c \int d\mathbf{r} \, \gamma(n_-(\mathbf{r})) n_+(\mathbf{r}) n_j(\mathbf{r}), \qquad (7)$$

and λ_j^{IPM} is the annihilation rate within the IPM ($\gamma \equiv 1$). Above, $n_j(\mathbf{r}) = |\psi_j(\mathbf{r})|^2$ is the electron density of the state j. In the state-dependent scheme the momentum density of a given (electron on a certain orbital) annihilating electron-positron pair is (apart from the factor γ_j) the same as in the IPM, i.e., the enhancement, which in a sense is averaged over the electron-positron pair, affects only the annihilation rate λ_j not the shape of the momentum distribution of the orbital j. Equation (5) is again satisfied. The problems related to the state-independent LDA scheme are avoided because the enhancement factor affects only the probability of annihilation of the positron with each electron state.

D. Projector augmented-wave method

1. Wave functions in the projector-augmented wave method

We use the projector augmented-wave (PAW) method[7] to describe the valence electron wave functions in solids. The PAW method is a full-potential all-electron method related both to the pseudopotential method and to the linearized augmented-plane-wave method (LAPW). It is based on a linear transformation between all-electron (AE) valence wave functions $|\Psi\rangle$ and soft pseudo (PS) valence wave functions $|\tilde{\Psi}\rangle$. The transformation can be written as (for details see Ref. 7)

$$|\Psi\rangle = |\tilde{\Psi}\rangle + \sum_i (|\phi_i\rangle - |\tilde{\phi}_i\rangle) \langle \tilde{p}_i | \tilde{\Psi} \rangle, \qquad (8)$$

where $|\phi_i\rangle$ and $|\tilde{\phi}_i\rangle$ are AE and PS partial waves localized around each nucleus and $\langle \tilde{p}_i |$ are soft, localized projector functions probing the local character of the PS wave function $|\tilde{\Psi}\rangle$. Index i stands for the site index R, the angular momentum indices (l, m) and an additional index k referring to the reference energy ε_{kl}. The solution of the self-consistent electronic structure for a given solid system means the solution of the PS wave functions. They are represented by plane-wave expansions in the Vienna *ab initio* Simulation Package[32–34] (VASP) which we are using. The construction of the AE wave functions in the PAW method is described in detail in Ref. 4. The AE valence wave functions are orthogo-

nal to the core states treated within the frozen-core approximation (free atom wave functions are used).

When calculating momentum distributions of annihilating electron-positron pairs, we construct the AE wave functions $|\Psi\rangle$ according to Eq. (8) in the Fourier space and then Fourier transform them to the real space. In the case of positrons localized at defects, the summation over R can be limited only to the atoms surrounding the defect. The positron state is solved in the real space. Then the products of the positron and electron wave functions are calculated and Fourier transformed [see Eq. (6)]. As a result we have a three-dimensional momentum distribution on the reciprocal lattice of the superlattice. Using a dense **k**-point mesh for electron wave functions we decrease the lattice constant in order to increase the momentum resolution and to get a converged result. Then, by integrating over the planes perpendicular to the chosen momentum distribution the Doppler spectrum is obtained with a sufficient resolution.

It is sufficient to use a typical value of about 250–400 eV for the kinetic energy cutoff of the plane-wave expansions when calculating the PS wave functions for the determination of the momentum distribution. The momentum components of the partial waves in Eq. (8) can be taken into account up to an arbitrary value p_{max}. We have found that the value $p_{max} = 70 \times 10^{-3} m_0 c$ is enough to guarantee that the Doppler spectrum [projection of $\rho(\mathbf{p})$ on the p_z axis] converges up to the momentum of $40 \times 10^{-3} m_0 c$, which is usually required when comparing results with coincidence Doppler broadening experiments.

The PAW method describes also the high-momentum Fourier coefficients of valence wave functions accurately, which is important when one compares theoretical results with experimental coincidence Doppler spectra. The efficiency and the flexibility of the method are also great benefits in the study of defects in solids. It also enables one to treat first-row elements, transition metals, and rare-earth elements.

2. Constructing the effective potential for the positron

Although the PAW method is an AE method, we do not in practice construct the AE valence charge density n in the three-dimensional real-space grid when constructing the effective potential for the positron or calculating the total annihilation rate λ. A sufficiently good approximation is to approximate n with $\tilde{n} + \hat{n}$, where $\tilde{n}$ is the PS valence charge density, calculated from the PS wave functions $|\tilde{\Psi}\rangle$, and $\hat{n}$ denotes the compensation charges as defined in Ref. 34. (Here we adopt the notation of Ref. 34.) The compensation charges $\hat{n}$ guarantee that the approximate Hartree potential due to the valence electrons, $v_H[\tilde{n} + \hat{n}]$, is equal to the AE Hartree potential $v_H[n]$ everywhere except near the nuclei, inside the localized compensation charges $\hat{n}$ ($r < r_{comp}^l$, where r_{comp}^l's are the cutoff radii of the compensation charges). The charge density $\tilde{n} + \hat{n}$ itself is correct outside the radii r_c^l ($> r_{comp}^l$), the cutoff radii for the partial waves $|\phi_i\rangle$ and $|\tilde{\phi}_i\rangle$, from nuclei. Typically the radii are, depending on the element, of the order of $r_c^l = 1.2, \ldots, 2.3 a_0$ and $r_{comp}^l = 0.8, \ldots, 2.0 a_0$, where a_0 is the Bohr radius (see Ref. 34).

Our approximation is justified by the fact that near the nuclei the positron density is vanishingly small because of the Coulomb repulsion of the nuclei. Thereby, the positron state is not considerably affected and the overlap of the electron and positron densities (the annihilation rate λ) does not appreciably change. Note, however, that we calculate $n_j(\mathbf{r})$, the charge density of the state j in Eq. (7) represented in the three-dimensional real-space grid, directly from the AE wave function $\psi_j(\mathbf{r})$.

After calculating the Coulomb potential due to both the valence and core electrons and nuclei, $v_H[\tilde{n} + \hat{n} + n_{Zc}]$, we calculate the electron-positron correlation potential and solve the positron state $\psi_+(\mathbf{r})$ in the effective potential $V_+(\mathbf{r})$ of Eq. (1) using the RQMG solver.[9] This is a fast and accurate method for our purpose where only the positron ground state corresponding to a rather smooth wave function in the interstitial region has to be solved.

E. Description of positron annihilation with core electrons

When modeling the positron annihilation and calculating momentum distributions of annihilating electron-positron pairs we describe the core electrons and the core electron charge density using atomic orbitals of isolated atoms calculated within the DFT and the LDA. In the calculation of the electron-positron pair wave function for the core electron Doppler spectrum we use an isotropic parametrized positron wave function[8] of the form

$$\psi_+(r) \approx C\{a_1 + [\text{erf}(r/a_2)]^{a_3}\}, \quad (9)$$

where C is a normalization factor and a_1, a_2, a_3 are parameters determined by fitting Eq. (9) to a spherically symmetric positron wave function calculated with the LMTO method within the atomic-spheres approximation (ASA). It is sometimes questionable to assume the positron wave function to be spherically symmetric around the nuclei when calculating the core electron Doppler spectrum. In the perfect bulk the positron wave function is very isotropic close to the nuclei. For the positron trapped by a vacancy-type point defect the decay of the positron wave function in the neighboring ion cores is similar to that in the bulk. The anisotropy around the nuclei causes extra localization in the positron-core-electron overlap, which causes some increase of the positron momentum which is omitted in the model. However, this is expected to be small in comparison with the positron momentum due to the decay toward the nuclei.

To test the effects of the frozen-core approximation and the isotropic positron wave function used when modeling the core-electron Doppler spectrum we have made two calculations for As vacancy (V_{As}) in GaAs by treating the $3d$ electrons of Ga first as valence electrons and then as core electrons. In the former calculation the full three-dimensional positron wave function is used in constructing the three-dimensional electron-positron pair wave functions corresponding to the Ga $3d$ electrons whereas in the latter calculation the positron wave function has the isotropic form of Eq. (9). The intensities of the results differ at high momenta due to the different degree of self-consistency but when one compares V_{As}/bulk ratios of Doppler spectra the results co-

incide. (As long as the $3d$ electrons of Ga are treated consistently in the bulk and defect calculations.)

F. Calculation of forces on ions due to a localized positron

When modeling relaxations of ions around vacancy defects the effects of the localized positron are included by using the so-called atomic-superposition (ATSUP) approximation[5] in which the charge density and the Coulomb potential are constructed from those of isolated atoms. In the CS the total energy is the sum of the total energy of the electron-ion system and the positron energy eigenvalue ε_+. Then the force due to the positron on ion j is the negative gradient of the positron energy eigenvalue ε_+ with respect to the position of the ion $\mathbf{R}_j$. According to the Hellman-Feynman theorem

$$\mathbf{F}_j^+ = -\boldsymbol{\nabla}_j \varepsilon_+ = -\boldsymbol{\nabla}_j \langle \psi^+ | H | \psi^+ \rangle = -\langle \psi^+ | \boldsymbol{\nabla}_j H | \psi^+ \rangle, \quad (10)$$

where the positron wave function $|\psi^+\rangle$ is assumed to be properly normalized. Within the ATSUP approximation and the LDA the effective potential for the positron [Eq. (1)] is of the form

$$V_+(\mathbf{r}) = \sum_j V_{\mathrm{Coul}}^{\mathrm{at},j}(|\mathbf{r}-\mathbf{R}_j|) + V_{\mathrm{corr}}\left(\sum_j n_-^{\mathrm{at},j}(|\mathbf{r}-\mathbf{R}_j|)\right), \tag{11}$$

where $V_{\mathrm{Coul}}^{\mathrm{at},j}$ and $n_-^{\mathrm{at},j}$ are the Coulomb potential and the charge density of the free atom j, respectively. Inserting this into Eq. (10) gives for the force

$$\mathbf{F}_j^+ = -\int d\mathbf{r}\, n_+(\mathbf{r})\left(\left.\frac{\partial V_{\mathrm{Coul}}^{\mathrm{at},j}(r)}{\partial r}\right|_{|\mathbf{r}-\mathbf{R}_j|} \right.$$
$$\left. + \frac{\partial V_{\mathrm{corr}}}{\partial n}\left.\frac{\partial n_-^{\mathrm{at},j}(r)}{\partial r}\right|_{|\mathbf{r}-\mathbf{R}_j|}\right)\frac{\mathbf{r}-\mathbf{R}_j}{|\mathbf{r}-\mathbf{R}_j|}. \tag{12}$$

The calculation of the positron-induced forces is fast within the ATSUP method. The forces are used with calculated electron-ion and ion-ion forces in order to find the relaxed ionic configuration of the defect. The ATSUP method itself does not give the possibility to study the relaxation of charged defects. However, if the positron state is solved in the self-consistent Coulomb potential instead of the superimposed potential of Eq. (11), the effect of the charge state comes into play, for example, in the case of negatively charged vacancies in semiconductors, via the stronger localization of the positron in comparison with the neutral vacancy, which will result in larger positron-induced forces. The approximations made when using Eq. (12) are tested below and compared with TCDFT results.

III. PERFECT BULK SYSTEMS

A. Testing the PAW method

We begin the testing of the PAW method for the calculation of momentum distributions of annihilating electron-positron pairs by comparing the results to those of the ATSUP approximation where atomic orbitals are used also
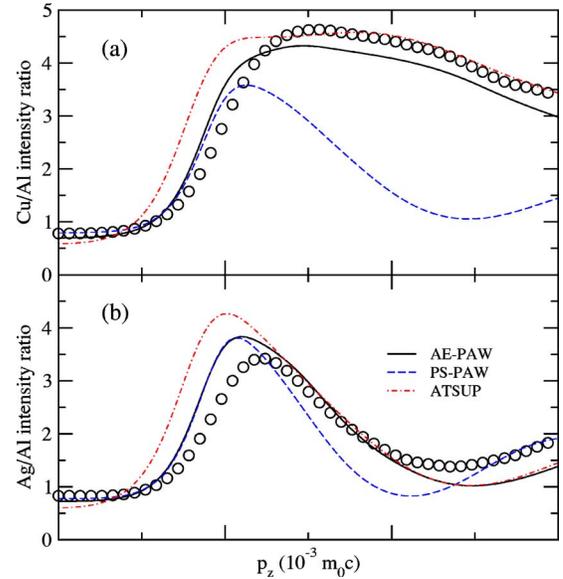
FIG. 1. (Color online) (a) Bulk Cu/bulk Al and (b) bulk Ag/bulk Al ratio curves of momentum distributions of annihilating electron-positron pairs calculated using the state-dependent scheme. The experimental data (Ref. 35) is shown with circles. The theoretical curves are convoluted with a Gaussian function with a FWHM of $4.3 \times 10^{-3}\ m_0 c$.

for valence electron states.[5] Here we also demonstrate the effect of the PAW transformation on the PS wave functions by showing also results calculated using only the PS wave functions of the PAW method. In the calculation of the electronic structures we employ the LDA exchange-correlation energy. The positron states and the annihilation characteristics are calculated within the BN-LDA.[6] The Doppler spectra are calculated using the state-dependent scheme.[8] The momentum distributions are finally convoluted with a Gaussian function with a full width at half maximum (FWHM) corresponding to the resolution of the Doppler experiment.

We have found out that a good way to compare theoretical and experimental Doppler spectra is to plot ratios to a reference spectrum. This way most of the systematic error is canceled. For the theoretical spectra this means especially that the overestimation of the core annihilation in the LDA is not a problem. In Fig. 1 we show our results for the ratios Cu/Al and Ag/Al calculated with the AE-PAW method, the PS wave functions of the PAW method and the ATSUP method compared to the experimental data from Ref. 35. In these calculations the Cu $3d$ and Ag $4d$ electrons are treated as valence electrons in the PAW calculations.

Due to the non-self-consistent construction of the valence electron wave functions the ATSUP method gives good results only at high momenta where the annihilation with the core electrons dominates. The results obtained with the AE-PAW method are clearly better in the low-momentum region of the spectra. In the high-momentum region these two results are equally good. The better compatibility of the crude ATSUP approximation with the experiment at high momenta in Fig. 1(a) may be just a coincidence. The PS wave functions of the PAW method fail to represent the high-frequency oscillations of the valence wave functions, especially those
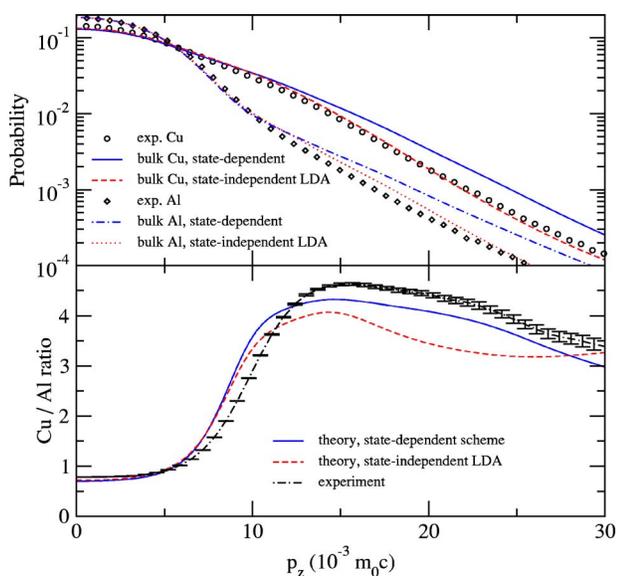
FIG. 2. (Color online) Bulk Cu/bulk Al ratio curve of momentum distributions of annihilating electron-positron pairs. The comparison between the state-dependent and the state-independent LDA schemes is shown. The experimental data is from Ref. 35. The theoretical curves are convoluted with a Gaussian function with a FWHM of 4.3×10^{-3} $m_0 c$.

FIG. 3. (Color online) Bulk Ag/bulk Al ratio curve of momentum distributions of annihilating electron-positron pairs. The comparison between the state-dependent and the state-independent LDA schemes is shown. The experimental data is from Ref. 35. The theoretical curves are convoluted with a Gaussian function with a FWHM of 4.3×10^{-3} $m_0 c$.

of the Cu $3d$ and Ag $4d$ electrons, in the core region although they predict the ratios well up to the momentum of about 10×10^{-3} $m_0 c$. The AE-PAW results in Fig. 1 are practically combinations of the ATSUP (at high momenta) and the PS-PAW (at low momenta) results. Because the quality of the PS-PAW results is comparable to calculations made using norm-conserving pseudowave functions[10,13] the tests made in this section clearly show the benefits of the use of the PAW method in the accurate calculation of momentum distributions of annihilating electron-positron pairs. We also note that positron lifetimes obtained for different bulk systems agree perfectly with previous all-electron results calculated with the same enhancement factor.

B. State-dependent scheme vs state-independent LDA scheme

In this section we compare the two above-mentioned ways to take into account the electron-positron correlation in the calculation of the momentum distribution of annihilating electron-positron pairs: the state-dependent scheme of Eq. (6) and the state-independent LDA scheme of Eq. (4). For simplicity, we use only bulk materials (Cu, Ag, Al, Si, Mo, and Fe) as examples. We use the experimental lattice constants and for Fe the experimental bcc structure. From now on we use the AE-PAW method within the frozen-core approximation.

We show in Figs. 2 and 3 the Doppler spectra of Cu, Ag, and Al calculated within the both above-mentioned schemes in the logarithmic scale and also normalize the Doppler spectra to the one of Al. The theoretical spectra and ratios are compared with the experimental ones by Nagai *et al.*[35] Both schemes describe the low-momentum region due to the annihilation with valence electrons well but the ratios tell, as
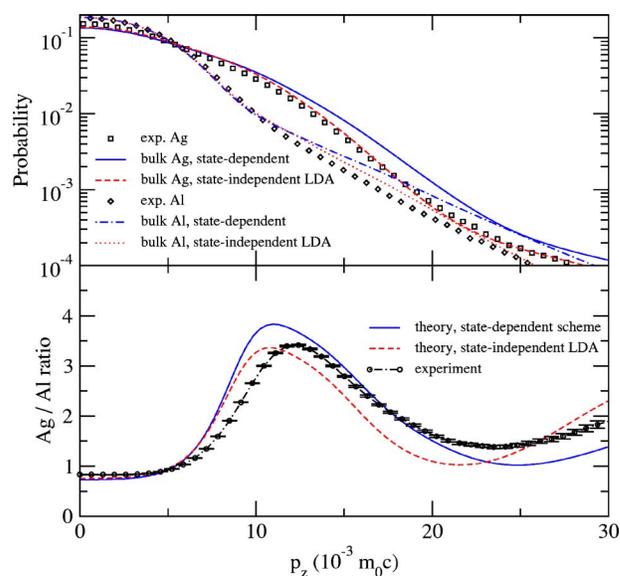
seen before,[8] that the state-independent LDA scheme fails to describe the high-momentum region of the Doppler spectra which arises from the annihilation with core electrons. The ratio Cu/Al (see Fig. 2) calculated using the state-independent LDA scheme is not even in a qualitative agreement with the experiment at high momenta. On the contrary, the state-dependent scheme describes the ratios quite accurately in both Figs. 2 and 3. However, when one looks at the absolute values of the spectra, the intensities at high momenta are in better agreement with the experiment in the results calculated using the state-independent LDA scheme but there is some unphysical oscillation in the spectra that does not exist in the state-dependent LDA results.

Further examples are shown in Figs. 4 and 5 where the Doppler spectra of Al, Si, Mo, and Cu are normalized to the one for Fe. For Fe we consider its magnetic ground state. The state-independent LDA fails again at high momenta, the result for Cu being again in the worst agreement with the experiment.

C. LDA vs GGA within the state-dependent scheme

In Figs. 4–7 we show similar comparisons between the BN-LDA and the GGA by Barbiellini *et al.*[26,27] The state-dependent scheme is used. The results calculated using the BN-LDA for the annihilation rates are in a better agreement with the experiment. In Figs. 6 and 7 the GGA tends to give too high values for the ratio at high momenta. In these particular examples the failure is mainly due to the large decrease of the relative core annihilation rate of Al calculated with the GGA compared to the one according to the BN-LDA. Because the state-dependent scheme is used the shapes of the contributions due to individual orbitals are the same
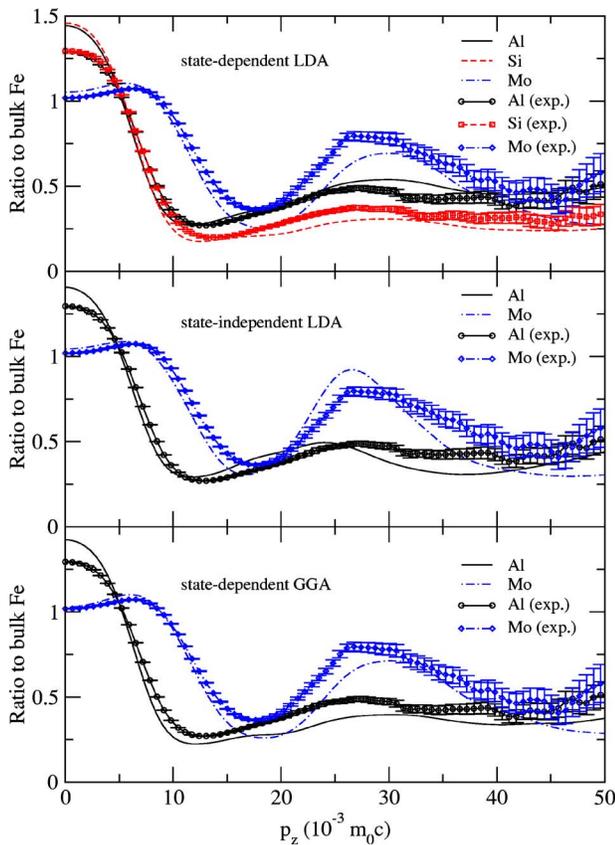
FIG. 4. (Color online) Ratio curves of momentum distributions of annihilating electron-positron pairs calculated using different approximations. The experimental data is from Ref. 36. The theoretical curves are convoluted with a Gaussian function with a FWHM of 4.7×10^{-3} $m_0 c$.

and also the shapes of the ratios are very similar. The ratios Al/Fe, Mo/Fe, and Cu/Fe calculated with the GGA are shown in Figs. 4 and 5. The results are in a rather good agreement with the experiment and only slightly worse than the ones calculated with the BN-LDA state-dependent scheme. The relative underestimation of the core annihilation in Al can be seen also in the ratio Al/Fe, which is lower at high momenta than the BN-LDA result. In contrast, as seen
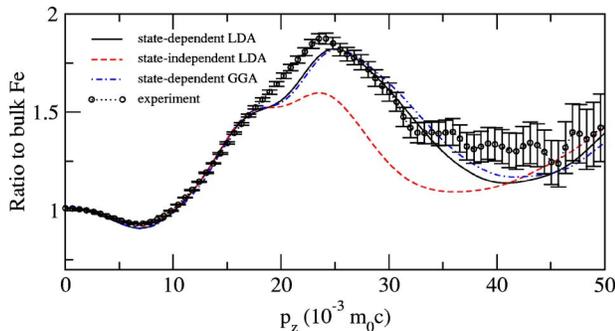
FIG. 5. (Color online) Bulk Cu/bulk Fe ratio curve of momentum distributions of annihilating electron-positron pairs calculated using different approximations. The experimental data is from Ref. 36. The theoretical curves are convoluted with a Gaussian function with a FWHM of 4.7×10^{-3} $m_0 c$.
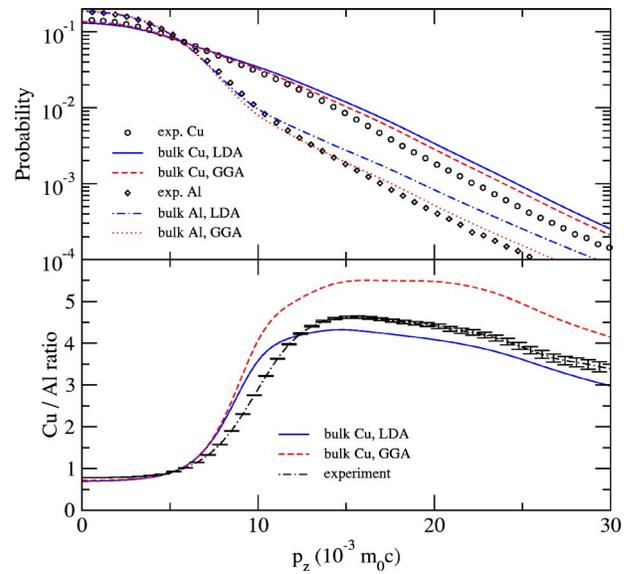
FIG. 6. (Color online) Bulk Cu/bulk Al ratio curve of momentum distributions of annihilating electron-positron pairs. The comparison between the BN-LDA and the GGA for annihilation rates within the state-dependent scheme is shown. The experimental data is from Ref. 35. The theoretical curves are convoluted with a Gaussian function with a FWHM of 4.3×10^{-3} $m_0 c$.

in Figs. 6 and 7 the GGA describes better the *absolute* intensities of the Doppler spectra because the annihilation rates of core orbitals are decreased.

The failure of the GGA in the ratios of Doppler spectra can be traced back to the semiempirical interpolation form of the GGA enhancement factor. Although its zero- and high-gradient limits are well defined the interpolation form is only
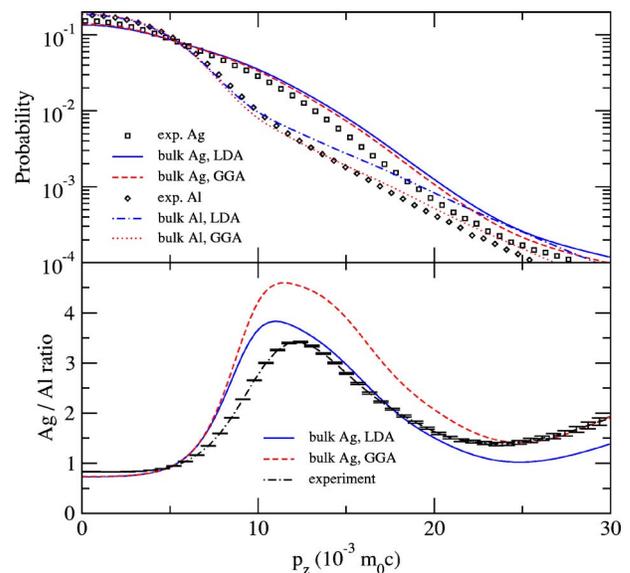
FIG. 7. (Color online) Bulk Ag/bulk Al ratio curve of momentum distributions of annihilating electron-positron pairs. The comparison between the BN-LDA and the GGA for annihilation rates within the state-dependent scheme is shown. The experimental data is from Ref. 35. The theoretical curves are convoluted with a Gaussian function with a FWHM of 4.3×10^{-3} $m_0 c$.

an approximation. Moreover, the free parameter α is just fixed to give *lifetimes* that are in good agreement with the experiment. Clearly, the BN-LDA succeeds to describe better the relative magnitudes of the annihilation rates λ_j between different electronic states and different elements.

We conclude that our choice for the approximation to be used with the state-dependent scheme is the BN-LDA because it gives better results than the GGA when comparing intensity ratios with the experiment. It is also simpler and more justifiable.

IV. VACANCY DEFECTS IN SOLIDS

The following step is to demonstrate that our scheme works also for positrons localized at vacancy-type defects. The CS has been shown to yield for a given ionic structure lifetimes[29] and also other annihilation characteristics[12] in good agreement with two-component calculations based on the Boroński-Nieminen formalism.

In this section we compare our results for vacancies in metals and semiconductors to experimental Doppler broadening results. We also study the effect of the positron-induced forces on ions neighboring vacancies. Further, we compare the ionic relaxations to previous two-component results and compare Doppler spectra calculated with the relaxed structures with experimental ones.

A. Relaxation tests

We study the effect of the localized positron on the relaxation of ions surrounding a vacancy by calculating the ionic structures of monovacancies in bulk Si, Al, and Cu with and without the localized positron. We consider first only isotropic relaxations. For Si we use a cubic 64-atom supercell and for Al and Cu cubic 108-atom supercells. In the electronic structure calculations we sample the Brillouin zone using 4^3, 8^3, and 6^3 Monkhorst-Pack[37] **k**-point meshes, respectively. Self-consistent LDA lattice constants are used in all calculations. We use the value 0.01 eV/Å as a stopping criterion for the forces on ions when finding the self-consistent ionic configurations.

We consider two different approximations for the force calculation. We solve the positron state either in the PAW potential or in the ATSUP potential. The first approximation is better in the sense that the positron density is able to follow the changes in the electronic structure but our force expression (12) is based on the ATSUP approximation and therefore the PAW potential is not consistent with the potential of the force calculation and thus the total energy minimum does not correspond to vanishing forces. In contrast, the latter more crude approximation is consistent with the force expression used and gives thus a well-defined and consistent total energy minimum.

The relaxations obtained with and without the positron are listed in Table I. The effect of the positron on the relaxations is clear; in all of these examples the inward relaxation is transformed to an outward relaxation due to the positron. The relaxations obtained with the PAW and the ATSUP potentials are very similar. We have studied the Si vacancy with the

TABLE I. Relaxations and corresponding positron lifetimes τ for monovacancies in different bulk materials. A positive (negative) number denotes the isotropic outward (inward) relaxation in percentage of the nearest neighbor distance with respect to the unrelaxed (ideal) vacancy. The table includes results calculated without the effect of the positron and with the positron state solved in the PAW/ATSUP potential. The relaxation is restricted to the symmetric breathing-mode relaxation. The numbers in parenthesis are calculated using a larger 216-atom supercell. Computed bulk lifetimes are 208 ps, 159 ps and 95 ps for Si, Al and Cu, respectively.

	no e^+		PAW		ATSUP	
	rel. (%)	τ (ps)	rel. (%)	τ (ps)	rel. (%)	τ (ps)
Si	−10.4	215	+5.6 (+11.3)	256 (272)	+5.9	257
Al	−1.7	219	+2.8	242	+2.9	251
Cu	−1.3	146	+2.4	163		

localized positron using also a larger cubic 216-atom supercell and only the Γ point. The results obtained are shown in Table I in parenthesis. The larger outward relaxation is explained by the fact that in the larger supercell the ions can relax more freely; interactions between periodic images of the vacancy are not as dominant as in the 64-atom supercell. In Fig. 8 we have plotted different energy components of the V_{Si} and V_{Al} systems as functions of vacancy relaxation relative to the relaxed geometry (ionic structure obtained including the effect of the forces due to the positron). Note, that one can not compare absolute energies between the results calculated with different potentials for the positron. The energy minimum for the PAW positron potential plus potential due to the electron-ion system is in both systems at about 1% smaller relaxation than the structure given by the relaxation (zero forces).

Our computational positron lifetimes for the monovacancies in Al and Cu are in good agreement with the experiment. The experimental lifetimes for V_{Al} and V_{Cu} are 251 ps (Ref. 38) and 179 ps (Ref. 39), respectively. They are high in comparison with the computed lifetimes since we use the LDA enhancement factor but we find a good agreement when we compare the vacancy-bulk lifetime differences with the experiment. (The experimental lifetimes for bulk Al and bulk Cu are 170 and 120 ps, respectively.[27]) The calculated and experimental results for the monovacancy in Si are compared in Sec. IV C.

B. Ga vacancy in GaAs

The triply negative Ga vacancy in GaAs has been extensively studied by Puska *et al.*[12] using the TCDFT and different schemes (including the CS) for the electron-positron correlation. Furthermore, also experimental coincidence Doppler broadening data exists.[40] Thus, using the Ga vacancy as a benchmark system, it is possible to compare simultaneously the relaxations and lifetimes obtained to two-component results and lifetimes and Doppler spectra to the experiment. We model the GaAs lattice using a cubic 64-atom supercell and sample the Brillouin zone in the
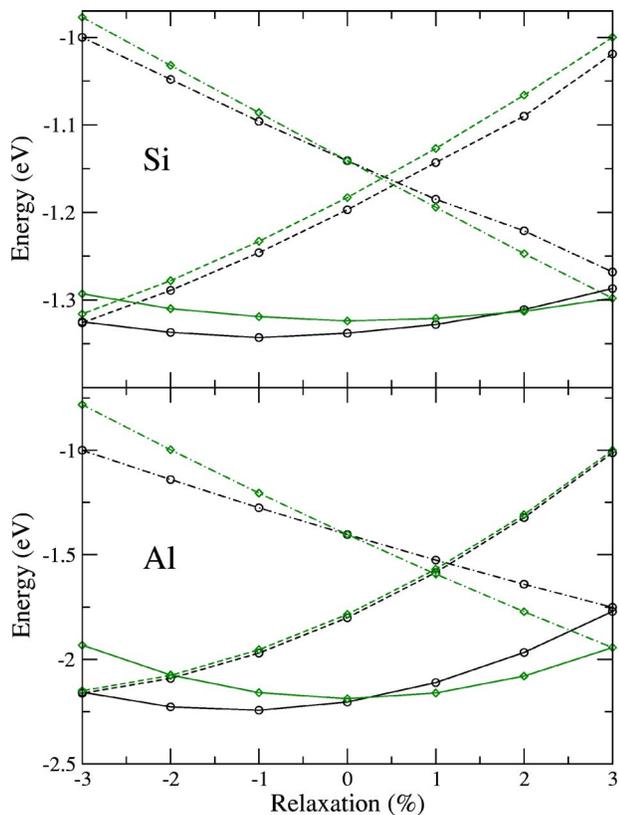
FIG. 8. (Color online) Different energy components as functions of vacancy relaxation in % of the nearest-neighbor distance (relative to the relaxed geometry, only nearest neighbor ions are moved) for V_{Si} in Si and V_{Al} in Al. The solid lines denote the total energy, the dashed lines the energy of the electron-ion system, and the dash-dotted line the positron energy eigenvalue. The figures show results in which the forces are calculated using a positron state solved in the PAW potential ($\bigcirc$) and in the ATSUP potential ($\diamond$).

electronic-structure calculations with a 4^3 Monkhorst-Pack **k**-point mesh.[37] In the case of the triply negative charge state of V_{Ga} all the localized states in the band gap are occupied and there is no symmetry lowering Jahn-Teller relaxation. By including the effect of the positron-induced forces on the relaxation we get an inward relaxation of 5.9% in very good agreement with the inward relaxation of 6.6% previously obtained using the two-component BN scheme.[12] In the work by Puska *et al.*[12] the authors did not calculate relaxations using the CS but showed that the total energy curves calculated as a function of the breathing-mode relaxations of the ions neighboring the vacancy using the the two-component BN and the CS nearly coincide. When this and the good agreement in relaxations are taken into account, one can conclude that our scheme for the calculation of forces gives very similar results to ones calculated using the two-component BN formalism.

In Fig. 9 we show the computed Doppler spectra (normalized to that of bulk GaAs) obtained for the relaxed structures of V_{Ga} in the charge states 3– and 1– compared with the experiment and the computed one for the neutral, ideal (unrelaxed) V_{Ga}. The corresponding relaxations and lifetimes are tabulated in Table II. Only isotropic relaxations have been considered using the small 64-atom supercell although a symmetry-breaking relaxation is expected for the 1- charge state. The agreement with the experiment both in the Doppler spectrum and in the lifetime (relative to the bulk one) is best for the 1- charge state. The inward relaxation for the 3– is too strong compared with the experiment because the lifetime and the ratio curve in Fig. 9 are too close to the bulk values.

We have also calculated the relaxation of V_{Ga}^{1-} using a larger cubic 216-atom supercell (with this supercell we use only the Γ point and do not treat the Ga $3d$ electrons as valence electrons). The calculation gives slightly smaller inward relaxation than that with the 64-atom cell. The results are given in Table II in parenthesis. We also break the T_d symmetry by displacing the nearest-neighbor atoms of the
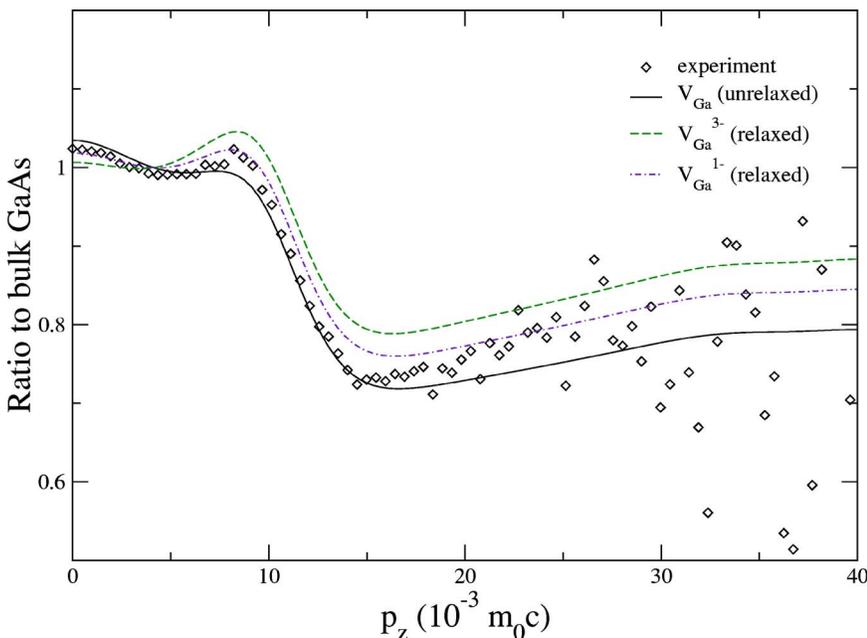
FIG. 9. (Color online) Theoretical ratio curves for the Ga vacancy in GaAs. The experimental data, measured from electron-irradiated GaAs, is from Ref. 40. The theoretical curves are convoluted with a Gaussian function with a FWHM of 5.5×10^{-3} $m_0 c$.

TABLE II. Relaxations and lifetimes for different charge states of V_{Ga} in GaAs. The numbers in parenthesis are calculated using a larger 216-atom supercell. The relaxation is restricted to the symmetric breathing-mode relaxation. A positive (negative) number denotes isotropic outward (inward) relaxation. The computed bulk GaAs lifetime is 208 ps.

defect	rel. (%)	τ (ps)	$\tau - \tau_{bulk}$ (ps)
unrel. V_{Ga}^0	0.0	249	38
V_{Ga}^{1-}	−2.8 (−2.3)	237 (244)	26 (33)
V_{Ga}^{3-}	−5.9	229	18
V_{Ga} [exp. (Ref. 41)]		260	30

vacancy in order to create a symmetry-breaking relaxation with the expected C_{2v} symmetry. The corresponding lifetime is 243 ps, which is almost the same as when assuming the T_d symmetry. (Note that Fig. 9 does not include any results calculated with the 216-atom supercell.)

The relative core annihilation rate (the experimentally measured relative W parameter, relative wrt bulk value) is sensitive to the treatment of the electron-positron correlation effects. The correlation potential used affects the degree of the localization of the positron and thereby the positron-core electron overlap and the core annihilation rate.[12] Puska *et al.*[12] obtained for the triply negative Ga vacancy in GaAs the values of 0.88 and 0.34 using the two-component BN formalism and the scheme by Gilgien *et al.*,[11] respectively. The computational values in the present work (estimated from Fig. 9) are of the order of 0.8 in good agreement with the experiment and the previous result obtained with the BN formalism. Our scheme has already previously been successful in describing the relative core annihilation rates in the case of Ga vacancy in GaN (Ref. 25) and monovacancy in Al.[24]

C. Neutral monovacancy in Si

The neutral monovacancy in Si is a very complex system with a flat potential-energy surface and several competing local minima as a function of ion positions.[42,43] One can get even qualitatively different results with two different approximations, e.g., for the exchange-correlation potential.[43] We study now the monovacancy in Si including the forces caused by the localized positron. We use the 216-atom supercell and the Γ point, begin from the structure obtained as a result from the isotropic relaxation (see Table II) and break the T_d symmetry by displacing the nearest-neighbor atoms of the vacancy in order to create a symmetry-breaking relaxation with the expected D_{2d} symmetry. We confirm the fact pointed out by several earlier studies[42–45] that a supercell with at least 216 atoms is needed in order to obtain a convergence with respect to the supercell size.
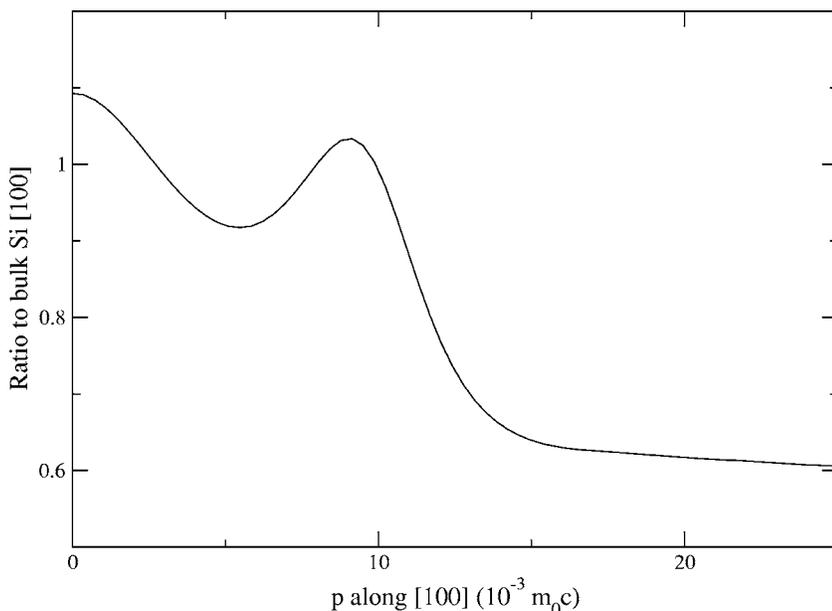
Our calculation gives an outward-relaxed structure with a slight D_{2d} symmetry. The corresponding lifetime is 270 ps; only 2 ps less than that for the vacancy constrained to the T_d symmetry. In Fig. 10 we show the obtained vacancy/bulk ratio of Doppler spectra. No experimental Doppler broadening data exists for the monovacancy in Si. Mäkinen *et al.*[46] and Polity *et al.*[47] obtained the positron lifetimes of 273 and 282 ps, respectively, for the monovacancy in Si created by electron irradiation. Taking into account that the calculated bulk lifetime with the LDA lattice constant used (208 ps) is lower than the experimental ones by Mäkinen *et al.* and Polity *et al.* (221 and 218 ps, respectively) we conclude that our result for the lifetime is in a good agreement with experiment.

Previously, Saito and Oshiyama[48] and Makhov and Lewis[45] have studied vacancies in Si within the two-component scheme by Gilgien *et al.*[11] including the effects of forces due to the positron. Their lifetimes for the monovacancy are reasonable but the relative W parameter of 0.28 estimated from Saito and Oshiyama's data is very low in comparison with our result, which is 0.72 (both evaluated using calculated annihilation rates as in Ref. 12).

V. SUMMARY AND CONCLUSIONS

In conclusion, we have presented an accurate scheme for the calculation of momentum distributions of annihilating

FIG. 10. Theoretical ratio curve for the neutral Si vacancy in Si. The the data is convoluted with a Gaussian function with a FWHM of $3.7 \times 10^{-3} \, m_0 c$

electron-positron pairs in solids based on the projector augmented-wave method. We have compared three commonly used approaches for the momentum distributions within the DFT framework. We have shown that the most appropriate way to take into account screening effects in the calculation of momentum distributions is to use a constant, state-dependent enhancement factor. Further, we have demonstrated that a position-dependent enhancement factor gives unphysical results when ratios of Doppler spectra are considered. The differences in results of the BN-LDA and the GGA by Barbiellini *et al.* is not large. Except for one of the studied elements (Al) the GGA gives comparable results. We choose to rely on the BN-LDA because of its simplicity and lack of semiempiric parameters. We underline that our choices are based on the theory-experiment comparison of ratios of momentum distributions for different materials rather than their absolute values. The latter may often be better described in the GGA and in the position-dependent enhancement schemes.

In addition to bulk solids our scheme is also reliable in the case of defects in materials. The comparison of our results for the Ga vacancy in GaAs to experiment suggests that the Ga vacancy seen in the experiment is negative but less than triply negative, which is the charge state suggested by a recent *ab initio* study.[49] For the neutral monovacancy in Si we have presented a prediction to be compared with future lifetime and coincidence Doppler broadening experiments.

*Electronic address: ima@fyslab.hut.fi

[1] R. Krause-Rehberg and H. Leipner, *Positron Annihilation in Semiconductors* (Springer-Verlag, Berlin, 1999).

[2] M. A. Coplan, J. H. Moore, and J. P. Doering, Rev. Mod. Phys. **66**, 985 (1994).

[3] *X-Ray Compton Scattering*, edited by M. J. Cooper, P. E. Mijnarends, N. Shiotani, N. Sakai, and A. Bansil (Oxford University Press, Oxford, 2004).

[4] I. Makkonen, M. Hakala, and M. J. Puska, J. Phys. Chem. Solids **66**, 1128 (2005).

[5] M. J. Puska and R. M. Nieminen, Rev. Mod. Phys. **66**, 841 (1994).

[6] E. Boroński and R. M. Nieminen, Phys. Rev. B **34**, 3820 (1986).

[7] P. E. Blöchl, Phys. Rev. B **50**, 17 953 (1994).

[8] M. Alatalo, B. Barbiellini, M. Hakala, H. Kauppinen, T. Korhonen, M. J. Puska, K. Saarinen, P. Hautojärvi, and R. M. Nieminen, Phys. Rev. B **54**, 2397 (1996).

[9] M. Heiskanen, T. Torsti, M. J. Puska, and R. M. Nieminen, Phys. Rev. B **63**, 245106 (2001).

[10] K. Saarinen, J. Nissilä, H. Kauppinen, M. Hakala, M. J. Puska, P. Hautojärvi, and C. Corbel, Phys. Rev. Lett. **82**, 1883 (1999).

[11] L. Gilgien, G. Galli, F. Gygi, and R. Car, Phys. Rev. Lett. **72**, 3214 (1994).

[12] M. J. Puska, A. P. Seitsonen, and R. M. Nieminen, Phys. Rev. B **52**, 10947 (1995).

[13] M. Hakala, M. J. Puska, and R. M. Nieminen, Phys. Rev. B **57**, 7621 (1998).

[14] S. Ishibashi, A. A. Manuel, M. Kohyama, M. Tokumoto, and H. Anzai, Phys. Rev. B **60**, R3747 (1999).

[15] T. Baruah, R. R. Zope, and A. Kshirsagar, Phys. Rev. B **60**, 10770 (1999).

[16] Z. Tang, M. Hasegawa, Y. Nagai, M. Saito, and Y. Kawazoe, Phys. Rev. B **65**, 045108 (2002).

[17] Z. Tang, M. Hasegawa, Y. Nagai, and M. Saito, Phys. Rev. B **65**, 195108 (2002).

[18] B. Barbiellini, S. B. Dugdale, and T. Jarlborg, Comput. Mater. Sci. **28**, 287 (2003).

[19] S. Ishibashi, A. A. Manuel, L. Hoffmann, and K. Bechgaard, Phys. Rev. B **55**, 2048 (1997).

[20] D. Vanderbilt, Phys. Rev. B **41**, R7892 (1990).

[21] S. Ishibashi, Mater. Sci. Forum **445–446**, 401 (2004).

[22] A. Uenodo, N. Hattori, H. Naruoka, S. Ishibashi, R. Suzuki, and T. Ohdaira, J. Appl. Phys. **97**, 023532 (2005).

[23] M. Rummukainen, I. Makkonen, V. Ranki, M. J. Puska, K. Saarinen and H.-J. L. Gossmann, Phys. Rev. Lett. **94**, 165501 (2005).

[24] A. Calloni, A. Dupasquier, R. Ferragut, P. Folegati, M. M. Iglesias, I. Makkonen, and M. J. Puska, Phys. Rev. B **72**, 054112 (2005).

[25] S. Hautakangas, I. Makkonen, V. Ranki, M. J. Puska, K. Saarinen, X. Xu, and D. C. Look (unpublished).

[26] B. Barbiellini, M. J. Puska, T. Torsti, and R. M. Nieminen, Phys. Rev. B **51**, R7341 (1995).

[27] B. Barbiellini, M. J. Puska, T. Korhonen, A. Harju, T. Torsti, and R. M. Nieminen, Phys. Rev. B **53**, 16201 (1996).

[28] J. Arponen and E. Pajanne, Ann. Phys. (N.Y.) **121**, 343 (1979).

[29] T. Korhonen, M. J. Puska, and R. M. Nieminen, Phys. Rev. B **54**, 15016 (1996).

[30] L. J. Lantto, Phys. Rev. B **36**, 5160 (1987).

[31] S. Daniuk, G. Kontrym Sznajd, A. Rubaszek, H. Stachowiak, J. Mayers, P. A. Walters, and R. N. West, J. Phys. F: Met. Phys. **17**, 1365 (1987).

[32] G. Kresse and J. Furthmüller, Comput. Mater. Sci. **6**, 15 (1996).

[33] G. Kresse and J. Furthmüller, Phys. Rev. B **54**, 11 169 (1996).

[34] G. Kresse and D. Joubert, Phys. Rev. B **59**, 1758 (1999).

[35] Y. Nagai, T. Honma, Z. Tang, K. Hono, and M. Hasegawa, Philos.

Mag. A **82**, 1559 (2002).

[36] Y. Nagai, Z. Tang, and M. Hasegawa, Radiat. Phys. Chem. **58**, 737 (2000).

[37] H. J. Monkhorst and J. D. Pack, Phys. Rev. B **13**, 5188 (1976).

[38] H. E. Schaefer, R. Gugelmeier, M. Schmolz, and A. Seeger, in *Proceedings of the Vth Risø International Symposium of Metallurgy and Materials Science*, edited by N. H. Andersen, M. Eldrup, N. Hansen, D. J. Jensen, T. Leffers, H. Lillholt, O. B. Pedersen and B. N. Singh (Risø National Laboratory, Risø, 1984).

[39] H. E. Schaefer, W. Stuck, F. Banhart, and W. Bauer, in *Proceedings of the 8th International Conference on Vacancies and Interstitials in Metals and Alloys*, edited by C. Ambromeit and H. Wollenberger (Trans Tech, Aedermannsdorf, 1986).

[40] T. Laine, K. Saarinen, J. Mäkinen, P. Hautojärvi, C. Corbel, L. N. Pfeiffer, and P. H. Citrin, Phys. Rev. B **54**, R11050 (1996).

[41] C. Corbel, F. Pierre, K. Saarinen, P. Hautojärvi, and P. Moser, Phys. Rev. B **45**, 3386 (1992).

[42] M. J. Puska, S. Pöykkö, M. Pesola, and R. M. Nieminen, Phys. Rev. B **58**, 1318 (1998).

[43] M. I. J. Probert and M. C. Payne, Phys. Rev. B **67**, 075204 (2003).

[44] C. D. Latham, M. Ganchenkova, R. M. Nieminen, S. Nicolaysen, M. Alatalo, S. Öberg, and P. R. Briddon, Phys. Scr. (to be published).

[45] D. V. Makhov and L. J. Lewis, Phys. Rev. B **71**, 205215 (2005).

[46] J. Mäkinen, C. Corbel, P. Hautojärvi, P. Moser, and F. Pierre, Phys. Rev. B **39**, 10162 (1989).

[47] A. Polity, F. Börner, S. Huth, S. Eichler, and R. Krause-Rehberg, Phys. Rev. B **58**, 10363 (1998).

[48] M. Saito and A. Oshiyama, Phys. Rev. B **53**, 7810 (1996).

[49] F. El-Mellouhi and N. Mousseau, Phys. Rev. B **71**, 125207 (2005).